IEEE Access
Multidisciplinary ⋮ Rapid Review ⋮ Open Access Journal

Received February 18, 2020, accepted February 25, 2020, date of publication March 2, 2020, date of current version March 13, 2020.

Digital Object Identifier 10.1109/ACCESS.2020.2977681

Disturbance Attenuation Predictive Optimal Control for Quad-Rotor Transporting Unknown Varying Payload

YUAN WANG[1], HONGMING CAI[2], JUNMIAO ZHANG[3], AND XUBO LI[4]

[1]Key Laboratory of Fundamental Science for National Defense-Advanced Design Technology of Flight Vehicle, Nanjing University of Aeronautics and Astronautics, Nanjing 210016, China
[2]School of Mechanical Engineering, Nanjing University of Science and Technology, Nanjing 210094, China
[3]School of Energy and Power Engineering, Jiangsu University of Science and Technology, Zhenjiang 212003, China
[4]Key Laboratory of Mechanics and Control of Mechanical Structures, Nanjing University of Aeronautics and Astronautics, Nanjing 210016, China

Corresponding author: Hongming Cai (chm@njust.edu.cn)

This work was supported in part by the Natural Science Foundation of Jiangsu Province, China, under Grant BK20160817, and in part by the Fundamental Research Funds for the Central Universities under Grant 30915118807 and Grant 30917011302.

ABSTRACT Quad-rotor is very suitable for payload transportation due to the merits of high maneuverability and free hovering. However, the unknown varying payloads can cause negative influences that act in forms of persistent disturbances and sudden changes, damaging flight performance especially the attitude stability seriously. Targeting the persistent disturbances, an entirely novel disturbance estimator (DE) which can estimate non-smooth disturbances in a highly accurate manner for feedback compensation is proposed in this paper. To deal with the sudden changes from prescribed references and the payloads that may induce too large overshoots and input surging, a type of predictive optimal controller, which considers tracking errors and their changing rates of a class of linear multiple-input-multiple-output systems, is developed. Simulation results show that the system enhanced by the DE has better control performance than the ones enhanced by the commonly used extended state observer or nonlinear disturbance observer. Compared with the typical control approaches, the proposed control scheme enables the quad-rotor attitude system more stable performance and more ideal inputs on both persistent disturbance and sudden change resisting during payload transportation.

INDEX TERMS Quad-rotor, payload transportation, disturbance attenuation, predictive optimal control.

I. INTRODUCTION

Recently, quad-rotors have been widely applied in many areas [1]–[3], due to their merits of high maneuverability, free hovering, and vertical take-off/landing. To meet the task requirements, many effective approaches were developed, such as proportional-integral-derivative (PID) [4], linear quadratic regulator (LQR) [5], model reference adaptive control (MRAC) [6], feedback linearization (FL) [7], sliding model control (SMC) [8], back-stepping (BS) [9], and disturbance observer-based control (DOBC) [10]–[20].

Among all applications of quad-rotors, payload transportation has gained more attentions [21]. Two connection methods are commonly used to connect the payload with a quad-rotor, namely the flexible connection (usually shown as cable-suspending) and the rigid connection (no relative movement between the payload and the quad-rotor, such as mechanism-fixing). Both of the two connection methods have their own application scenarios and advantages. But, according to the references reviewed by the authors, existing researches mainly focused on the control of quad-rotor with flexible connection and dedicated to reduce oscillation caused by swing angle between the suspended stuff and the aircraft [22]–[32]. Only a few literatures studied flight control of the quad-rotors using rigid-connection and mainly focused on the unknown masses of the payloads. In [33], an adaptive fractional order sliding mode control approach with mass estimation mechanism was proposed for the quad-rotor transporting time-varying payload. Wang *et al.* [34] developed an integral sliding mode based adaptive robust control algorithm to control a quad-rotor helicopter transporting payload with unknown mass. Sadeghzadeh *et al.* [35] studied

The associate editor coordinating the review of this manuscript and approving it for publication was Mou Chen.

payload dropping (airdrop) application of a quad-rotor helicopter using a gain-scheduled PID method and a model predictive control method. Shastry *et al.* [36] used a nonlinear adaptive control method to manipulate the automatic delivery system of a quad-rotor. Pratama *et al.* [37] employed a PD controller to stabilize a quad-rotor in the mission of unknown payload transportation; the uncertain inertia perturbation from payloads was considered. In [38], a linear matrix inequality-based nonlinear adaptive robust control approach was proposed for the quad-rotor delivering packages with unknown masses in the presence of wind field. In [39], [40], multiple quad-rotors were applied to transport payloads with each one controlled by PID controllers. In [41], a quad-rotor equipped with a two degree-of-freedom robotic arm was used to deliver payloads to remote places. The SMC approach was used to prevent the aircraft from influences induced by unknown payloads. From the perspective of the authors, though the flexible connection is suitable for the payloads with different sizes and shapes, the rigid one is more stable and safety (payload swinging is easy to happen in flexible connection, causing instability of altitude/attitude and collision between the payload and the aircraft) during mission execution. These lead us to focus on the flight control of quad-rotors transporting payloads using the rigid connection.

During the period of payloads transportation, attitude control plays a decisive role in stable flight, accurate delivery, and precise path following. However, this is a challenging task. When the payload is empty, attitude dynamic system of the quad-rotor is originally highly nonlinear. The pitch, roll, and yaw torques can approximately be decoupled because of the nearly symmetric frame structure (mathematically the inertia matrix is diagonal) [10], [33], [43], [45], [46], [48], [51]. However, when the unknown payload is loaded using rigid connection, symmetry of the quad-rotor is broken such that the inertia matrix becomes non-diagonal, which in turn results in couplings among the pitch, roll, and yaw torques. Besides, due to the existence of eccentricities (can be seen in Fig. 8 in next) between the gravitational centers of the payload and the aircraft, the quad-rotor is affected by uncertain disturbance torques from overweight of the payload. Based on above analyses, uncertainties, nonlinearities, and couplings in the attitude system are all significantly escalated after loading the payloads. Hence, studying the attitude control of the quad-rotor in this situation is necessary and of significance in engineering. Meanwhile, this study also enriches researches for this application.

Although the aforementioned approaches have been applied to the quad-rotor with or without transporting payloads, they have their own flaws or are based upon assumptions. For example, control schemes based on the PID and LQR methods cannot guarantee the closed-loop performance in different flight conditions. In the MRAC approach, finding a reference model is usually a challenging mission. As for the FL method, detailed plant model information is required, resulting in poor system robustness against uncertainties. The sliding mode controller is insensitive to uncertainties and can stabilize the system globally. However, to achieve good system robustness against uncertainties, the accurate upper bound (UB) of the amplitude of the uncertainties must be available. Practically, the accurate UB may not be obtained easily. Hence, an overestimation of the UB is usually used, resulting in high-frequency of both switching of the control input and chattering around sliding mode surface. This possibly degrades the control performance and negatively affects the actuator. The conventional BS method can only deal with the constant or slowly changing uncertainties. Though disturbance observers such as the extended state observer (ESO) and the nonlinear disturbance observer (NDO) have been proved to be effective to improve flight performance of the quad-rotor systems, they show poor capability on the estimation of non-smooth disturbances.

Motivated by the previous works, this paper proposes a novel control scheme with disturbance attenuation and prediction functions for attitude stabilization of the quad-rotor transporting payloads. Firstly, the rotational dynamic system is modeled as two cascade multiple-input-multiple-output (MIMO) systems. Secondly, an entirely novel disturbance estimator (DE) is proposed to deal with the non-smooth disturbances. Thirdly, we develop a modified predictive functional controller to deal with the sudden changes from prescribed references and external disturbances. Finally, validation of the proposed control scheme is carried out through numerical simulations.

The rest part of this paper is organized as follow: Section II summarizes scope and main contributions of this paper. Section III proposes a novel DE and shows its stability analysis. Section IV develops a predictive optimal controller for linear MIMO systems. Section V builds the plant model of the quad-rotor carrying payloads. Section VI designs control scheme for the quad-rotor delivering payloads. Section VII conducts contrast simulations to validate superiority of the proposed control scheme. Finally, some conclusions are drawn in Section VIII. One online estimation algorithm and proofs of four theorems are presented in appendixes.

II. PAPER SCOPE AND CONTRIBUTION

This paper investigates the attitude stabilization problem of the quad-rotor transporting unknown and varying payloads using a disturbance attenuation predictive control scheme. The payload connected with the quad-rotor using a fixed connection method rather than cable-suspended methods is considered. Main contributions are summarized as:

1. In the control design, a MIMO system-based disturbance estimation and control technique is proposed. The control structure is simpler than the ones decoupling the quad-rotor system into several single-input-single-output (SISO) subsystems [10], [11], [13]–[17], [19], [20], [42]–[48].
2. We consider more elements such as unknown moments of inertia, disturbance torques, and sudden changes causing negative influences, which is more comprehensive and

practical than existing studies [33], [34], [38] that only took into account of the unknown weights.

3. We propose a novel DE suitable for a class of MIMO systems to estimate the non-smooth disturbances in an accurate manner by means of the compact form dynamic linearization (CFDL) theory [49]. The work is original rather than an extension of the previous works and extends the application ranges of the existing DOs [50]–[55] significantly. Superiority of the DE can be seen in Section III, part F, by making comparison with the commonly used extended state observer (ESO) [50], [54] and nonlinear disturbance observer (NDO) [50], [55].
4. We develop a new predictive optimal controller (POC) to degrade impacts from sudden changes. The POC has better capability on output overshoot restraint compared with conventional predictive approaches whose control performances mainly depend on the length of predictive horizon (LPH) [56]–[60]. The predictive function has been proved to be effective to deal with sudden changes [61].

III. DISTURBANCE ESTIMATION

In this section, some notations used in the rest part of this paper is introduced firstly. Then two assumptions and one important lemma as preliminaries for obtaining the DE are introduced. After deriving the formulation of the DE, we analyze its stability and illustrate its superiority by making comparison with the aforementioned ESO and NDO.

A. MATHEMATICAL NOTATIONS

Denote T as sampling period; $S(kT) \triangleq S(k)$, S is a scalar or vector, k is a positive integer; $\Delta S(k+1) \triangleq S(k+1)-S(k)$; $\|(\cdot)\|$ represents matrix norm; $\|(\cdot)\|_v$ represents the compatible norm of a matrix; $\widehat{S}(k)$ represents the estimation of $S(k)$ at time point kT; $diag(a_1, \cdots, a_n)$ denotes a $n \times n$ diagonal matrix with diagonal elements $a_1, \cdots, a_n$; $S(k+i|k)$ represents prediction of S at time point $(k+i)\,T$ based upon $S(k)$.

B. PRELIMINARIE

In this subsection, we consider the following general MIMO nonlinear system:

$$\Sigma_1 : Y(k+1) = f(Y(k), \cdots, Y(k-n_y+1), U(k), \cdots, U(k-n_u+1)) \quad (1)$$

where, $U(k) \in R^m$ and $Y(k) \in R^m$ are measureable input and output signals at sampling time point k; n_y and n_u are two integers; $f(*) = [f_1(*), \cdots, f_m(*)]^T$ is a nonlinear mapping vector.

Two assumptions are made for system Σ_1:

(A1): The partial derivatives of $f_i(*)$, $i = 1, \cdots, m$ with respect to every entry of the $(n_y+1)^{\text{th}}$ variable $U(k)$ are continuous.

(A2): System Σ_1 satisfies the generalized Lipschitz condition. That is,

$$\|Y(k_1+1) - Y(k_2+1)\| \le b_c \|U(k_1) - U(k_2)\|$$

for any $k_1 \ne k_2$, $k_1 \ge 0$, $k_2 \ge 0$ and $U(k_1) \ne U(k_2)$. Where, b_c is a bounded positive number.

Lemma 1 [49]: Consider that system Σ_1 satisfies A1 and A2. If $\|\Delta U(k)\| \ne 0$ for any k, then there exists a time-varying diagonally dominant matrix $\Phi_c(k) \in R^{m\times m}$ called pseudo Jacobian matrix (PJM), such that system Σ_1 can be transformed into the following compact form dynamic linearization (CFDL) data model:

$$\Delta Y(k+1) = \Phi_c(k) \cdot \Delta U(k) \quad (2)$$

Proof of this lemma can also be seen in [49]. It is impossible to obtain analytical solution of $\Phi_c(k)$ since it is time-varying and includes all system nonlinearities. In [49], many methods were adopted to estimate the PJM. For simplicity, one of the estimation algorithms is given in Appendix A directly.

Remark 1: Assumption 2 and formula (2) imply that $\|\Phi_c(k)\| \le b_c$.

C. DESIGN OF THE DISTURBANCE ESTIMATO

To get into the details of the design work, follow general continuous MIMO affine nonlinear system is considered:

$$\overline{\Sigma}_1 : \dot{Y} = H(Y, U) + B \cdot U \quad (3)$$

where, $U = [u_1, \cdots, u_m]^T \in R^m$ and $Y = [y_1, \cdots, y_m]^T \in R^m$ are measureable input and output vectors, respectively; $B \in R^{m\times m}$ is full rank; $H(*) = [h_1(*), \cdots, h_m(*)]^T$ is an unknown nonlinear mapping vector and $h_i(*)$, $i = 1, \cdots, m$ are not limited to the smooth type like in [50].

A forward difference-based discrete-time form of system $\overline{\Sigma}_1$ using sampling period T is given by:

$$\Sigma_p : Y(k+1) = Y(k) + T \cdot H(Y(k), U(k)) + T \cdot B \cdot U(k) \quad (4)$$

System (4) also satisfies A1 and A2. In next, Σ_p is called plant model.

Remark 2: System (3) or (4) represents a series of dynamic systems. Typical examples are attitude dynamic systems of fixed-wing airplanes, multi-rotor aircrafts, space crafts and vessels.

Generally, the fundamental ideal of disturbance estimation for existing DOs can be stated as: for a disturbed plant model, select an appropriate nominal model without uncertainties. Then use states and outputs of both the plant model and the nominal model to reconstruct the disturbance terms through algorithms.

In this paper, a nominal model relative to the plant model (4) is given by:

$$\Sigma_m : \; Y_m(k+1) = Y_m(k) + T \cdot B_m \cdot U(k) \quad (5)$$

where, $Y_m \in R^m$; $B_m \in R^{m\times m}$ is a full rank matrix, which is the estimation of B.

The disturbance terms need to be estimated are given by:

$$G(k) = H(Y(k), U(k)) + (B - B_m) \cdot U(k) \quad (6)$$

Let $\varepsilon(k) = Y(k) - Y_m(k)$. One of our main results is given in Theorem 1. Proof of Theorem 1 is given in Appendix B.

Theorem 1: Consider a class of disturbed MIMO system shown in (3) or (4) satisfying A1 and A2. By selecting a nominal model (5), then at any sampling time point kT, there must exist a time-varying diagonally dominant matrix $\widehat{\Phi}_c(k)$ such that estimation of the disturbance terms (6) can be derived by follow disturbance estimator:

$$\widehat{G}(k) = \frac{\Delta\varepsilon(k)}{T} + \widehat{\Phi}_c(k) \cdot \Delta U(k) \tag{7}$$

Remark 3: Compensating the plant model Σ_p into the nominal model Σ_m is reasonable and can usually be seen in flight control of aircrafts. In the conventional nonlinear dynamic inversion (CNDI) approach [62]–[64], modeling values of the nonlinear terms were used to compensate the nonlinear terms. While in [44], [65], values of the nonlinear terms were estimated by the DOs rather than from modeling such that the CNDI was modified dramatically.

Remark 4: It can be noticed that the proposed DE only requires the disturbance terms to satisfy A1 such that the drawback 'smooth' is overcome by means of the CFDL.

D. STABILITY ANALYSIS

One of the main issues in disturbance estimation is whether or not the difference between the real value and the estimation under the derived disturbance estimator/observer is convergent. The stability result is given in Theorem 2. Proof of Theorem 2 is given in Appendix C.

Theorem 2: For the system (3) or (4), the estimation error of the disturbance term between the real value (6) and the estimated value (7) from the proposed DE under the given nominal model (5) is bounded.

E. PARAMETER TUNING RUL

In this subsection, we aim to give qualitative tuning rules for the parameters of the DE in Appendix A. Except for their prescribed ranges which have been listed in the appendix, follow tuning rules deriving from our tuning experiences from applications are introduced.

1. $\mu > 0$ is one of the most important parameters that would affect convergence of the DE. A large value of μ has a trend to accelerate convergence speed of the PJM $\widehat{\Phi}_c(k)$ and restrain fluctuations at sudden change points of the disturbances.
2. Initial value of the PJM $\widehat{\Phi}_c(k)$, namely, $\widehat{\Phi}_c(0)$, is another most important parameter affecting convergence of the DE. $\widehat{\Phi}_c(0)$ is always selected as a diagonal matrix with diagonal elements $\widehat{\phi}_{ii}(0), i = 1, \cdots, m$. Small values of $\left|\widehat{\phi}_{ii}(0)\right|$ are beneficial to restrain fluctuations at non-smooth points of disturbances. Large values would result in DE instability. We suggest giving the $\left|\widehat{\phi}_{ii}(0)\right|$ small values (their signs are not important). For example, values less than 0.01 or 0.001 or even smaller will be fine.
3. The determinations of η, α, and b_1 have great arbitrary even for different systems. They only have to follow: $\eta \in (0, 2]$, $\alpha \geq 1$ and $b_1 > 0$.

TABLE 1. Comparison result with the conventional ESO And NDO.

Name	System scope	Disturbance scope
Proposed DE	SISO, MIMO	Smooth, Non-smooth
Conventional ESO	MISO	Smooth
Conventional NDO	SISO, MIMO	Smooth

F. ESTIMATION CAPABILITY VALIDATION

Though drawbacks of the conventional ESO and the NDO have been introduced in the Introduction part, this subsection highlights the superiority of the DE compared with the two DOs through simulations intuitively. Firstly, the comparison results are summarized in follow table.

As for the NDO, although it can overcome the drawbacks to some extent through tuning parameters, it is hard to determine its control parameters/functions.

Secondly, to validate effectiveness of the DE, we take follow linear system as example:

$$\dot{x} = u + d(t)$$

where, u represents the input. x represents the state as well as the output. $d(t) = 10sign[\sin(0.5\pi t)]$ represents the disturbance, $sign(*)$ is the symbol function. It is necessary to emphasize that setting the amplitude of $d(t)$ as 10 is only to make clear understanding of the validation effects. Besides, to make the comparisons more apparent, amplitude limitation of the outputs is not adopted.

The rest task is to design a control scheme such that the system can track a given prescribed reference y_d. One simple candidate controller is given by:

$$u(k) = \omega\left[y_d(k) - x(k)\right] - \widehat{d}(k)$$

where, ω is a tuning parameter called controller gain, $\widehat{d}(k)$ is the estimation of d at the sampling time point kT.

In next, $\widehat{d}(k)$ is given by the DE, ESO, and NDO, respectively, to validate the superiority of the DE. Initial conditions are given by: $\widehat{d}(0) = 0, x(0) = 0$. Parameters of the ESO and the NDO are tuned to optimal such that the response times at the non-smooth points for observing the disturbances are as short as possible. Contrast results of responses of unit-step prescribed reference are shown as:

Figure 1 illustrates that, by using the same controller gain, control performance based upon the DE is significantly superior to the ones based on the ESO and NDO since overshoots of the lateral two are up to 25% compared with 4% of the DE. The reason is that, in right neighborhoods of the non-smooth points ($t = 1$ and $t = 3$), the proposed DE can estimate the disturbance accurately, while the ESO and NDO cannot, as shown in Figure 2. Hence, errors between real value and estimation of the disturbance using the ESO and NDO are so large that system input must surge to suppress the disturbance and guarantee system stability, which in turn results in the overshoot of system output, as shown in Figure 1 and Figure 3. Figure 4∼ Figure 7 show

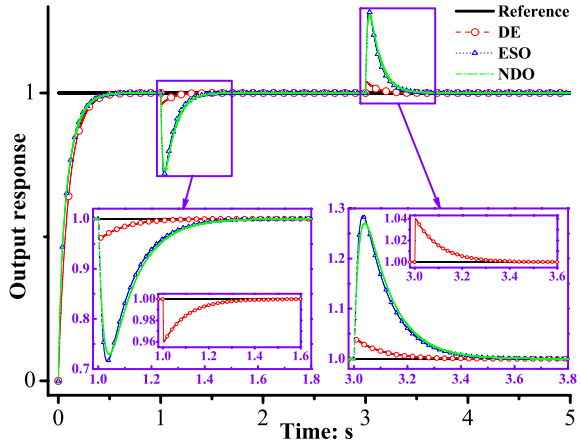

FIGURE 1. Comparison of system output: $\omega = 10$.

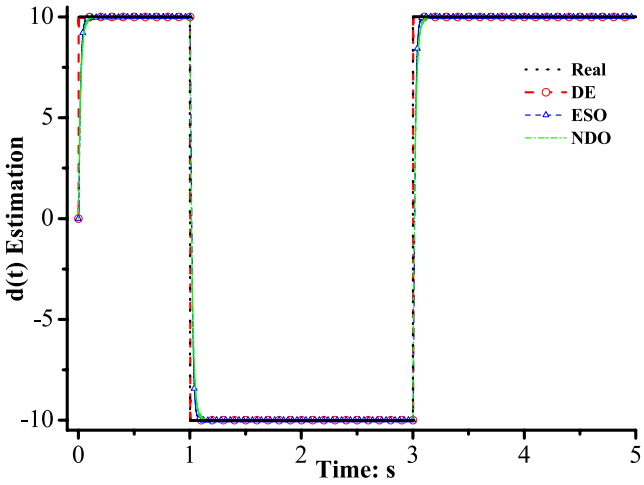

FIGURE 2. Disturbance estimation: $\omega = 10$.

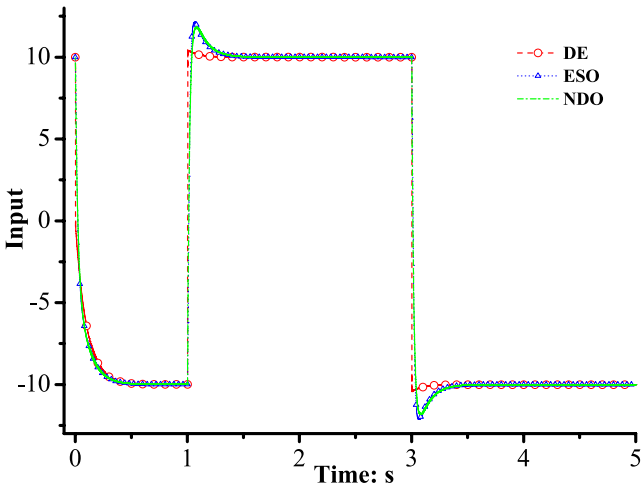

FIGURE 3. System input: $\omega = 10$.

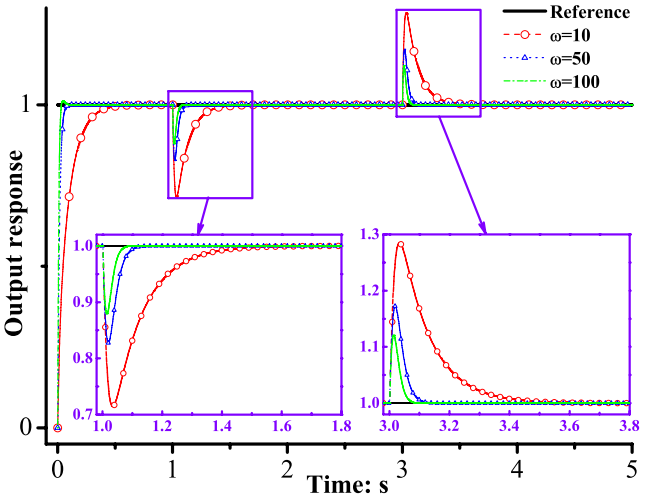

FIGURE 4. ESO-based system output: different ω.

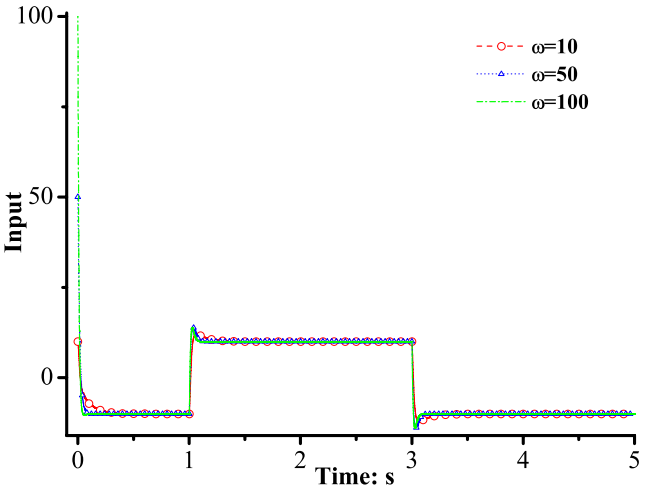

FIGURE 5. ESO-based system input: different ω.

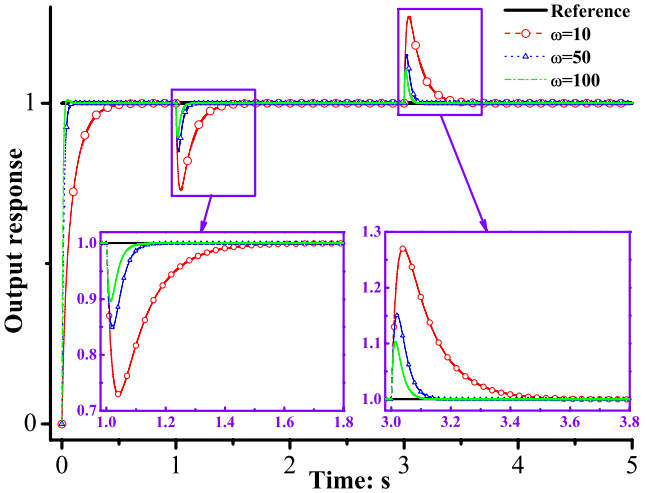

FIGURE 6. NDO-based system output: different ω.

that, increasing amplitude of the controller gain ω is beneficial to reduce output overshoots. However, this would cause severe input surging, especially in initial period of the simulation.

IV. PREDICTIVE OPTIMAL CONTROL FOR MIMO SYSTEM

During the payload transportation, sudden changes usually exist such that input surging/saturation and large output overshoot may occur, damaging flight performance of the

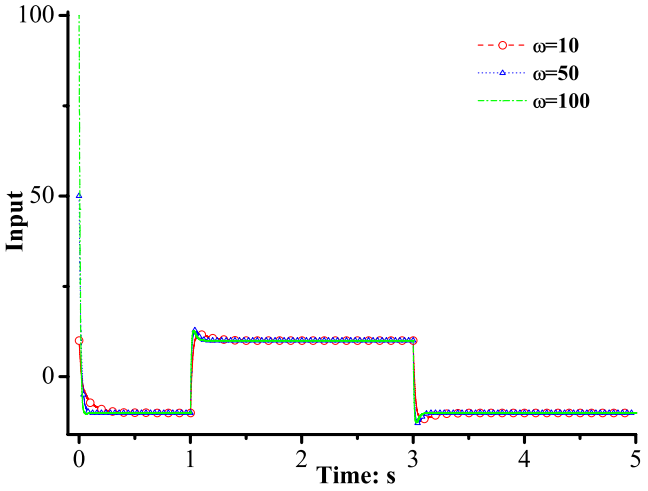

FIGURE 7. NDO-based system input: different ω.

quad-rotor. For example, the piecewise prescribed references with jumping points bring sudden changes. Besides, loading and dropping periods of the payloads are so short that the external disturbance forces and torques acting on the quad-rotor change quite fast. This would also be treated as a type of sudden change. This section develops a novel predictive controller to degrade the influences from the sudden changes, with stability of the closed-loop system analyzed.

A. REVIEW OF CONVENTIONAL PREDICTIVE APPROACH FOR LINEAR MIMO SYSTEM

In this subsection, we review the design of conventional predictive functional controller (PFC) which is the basis for the proposition of our controller. To make the work clear here, we consider the plant model (4) and the nominal model (5). Notice in Theorem 2 that the error between the real value and the estimation of the disturbance is non-zero. Thus, outputs of the two models are not the same, namely, $Y(k) \neq Y_m(k)$. In the conventional PFC, to minimize the output error such that the nominal model can be used to design controllers, a receding-horizon feedback correction approach is adopted and is stated as: design a controller considering the output error $Y(k) - Y_m(k)$, such that the closed-loop system is asymptotically stable and the output, $Y(k)$, of the system (5) optimally tracks a prescribed reference, $Y_d(k) = [y_{1d}(k), \cdots, y_{md}(k)]^T$, at any sampling point kT, in terms of a given performance index.

According to [66], following predictions of the input signal and the output error are adopted:

$$U(k+i|k) = U(k), \quad 1 \le i \le n \tag{8}$$

$$\begin{cases} \varepsilon(k) = Y(k) - Y_m(k) \\ \varepsilon(k+i|k) = \varepsilon(k), \end{cases} \quad 1 \le i \le n \tag{9}$$

The output in receding-horizon is predicted by linear recursion. Applying recursion to the nominal model (5) and using formula (8) yield:

$$\begin{cases} Y_m(k+1|k) = Y_m(k) + T \cdot B_m \cdot U(k) \\ Y_m(k+2|k) = Y_m(k+1|k) + T \cdot B_m \cdot U(k+1|k) \\ \qquad\qquad = Y_m(k) + 2T \cdot B_m \cdot U(k) \\ \qquad \vdots \\ Y_m(k+n|k) = Y_m(k+n-1|k) + T \cdot B_m \cdot U(k+n-1|k) \\ \qquad\qquad = Y_m(k) + nT \cdot B_m \cdot U(k) \end{cases} \tag{10}$$

By bringing formula (9) into (10), output prediction of the plant model (4) is given by:

$$\begin{aligned} Y(k+n|k) &= Y_m(k+n|k) + \varepsilon(k+n|k) \\ &= Y_m(k) + nT \cdot B_m \cdot U(k) + Y(k) - Y_m(k) \\ &= Y(k) + nT \cdot B_m \cdot U(k) \end{aligned} \tag{11}$$

To derive an optimal controller, follow receding-horizon performance index is usually adopted:

$$\begin{aligned} J(k) = \frac{1}{2} &[Y_d(k+n|k) - Y(k+n|k)]^T \\ &\times [Y_d(k+n|k) - Y(k+n|k)]^T \end{aligned} \tag{12}$$

where, $Y_d(k+n|k) = [y_{1d}(k+n|k), \cdots, y_{md}(k+n|k)]^T$.

Then according to the necessary condition for the existence of extrema, namely, $\partial J(k) \big/ \partial U(k) = 0$, the control law can be derived and is given by:

$$U(k) = (nT \cdot B_m)^{-1} [Y_d(k+n|k) - Y(k)] \tag{13}$$

B. THE PROPOSED PREDICTIVE OPTIMAL CONTROLLER

Notice that the receding-horizon performance index (12) only considers output tracking error such that the output overshoot would occur when the system encounters sudden changes. To deal with this problem, a novel receding-horizon performance index considering output tracking error and its changing rate is developed:

$$\begin{aligned} J(k) &= \frac{1}{2} S^T(k+n|k) S(k+n|k) \\ &\begin{cases} S(k+1) = C \cdot E(k+1) + \dfrac{E(k+1) - E(k)}{T} \\ E(k) = Y_d(k) - Y(k) \end{cases} \end{aligned} \tag{14}$$

where, n represents the length of predictive horizon. $C \in R^{m \times m}$ is an adjustable positive definite diagonal matrix.

It can be seen that index (14) considers both tracking error and its changing rate such that the output can track the prescribed reference accurately and would not change severely in the meanwhile.

In next, the rules (8) and (9), the output prediction (11), and the receding-horizon feedback correction are combined with formula (14) to derive our controller. Another one of our main results is given in Theorem 3. Proof of Theorem 3 is given in Appendix D.

Theorem 3: Consider that a class of disturbed nonlinear MIMO system (4) can be compensated into the given nominal model (5). Then for a given definite diagonal matrix C, the predictive optimal control law which minimizes the receding horizon performance index (14) is given by:

$$U(k) = [(nT \cdot C + I)B_m]^{-1}\left[\overline{Y}_d(k+n|k) - C \cdot Y(k)\right] \quad (15)$$

where, $\overline{Y}_d(k+n|k)$ is given by:

$$\overline{Y}_d(k+n|k) = (C + \frac{1}{T}I)Y_d(k+n|k) - \frac{1}{T}Y_d(k+n-1|k) \quad (16)$$

It is obvious that $Y_d(k+i|k)$, $1 \le i \le n$ are available and $\overline{Y}_d(k+n|k)$ can be computed offline in advance.

C. PARAMETER TUNING RUL

In this subsection, firstly, we describe functions of each parameters (the LPH n and the penalty factor C) in controller (15) qualitatively. Secondly, we give tuning rules for them step by step.

Function description:

Small values of n and large values of C would result in fast response speed, short response time, and large amplitude of inputs. The output overshoots are restrained effectively by the factor C.

Tuning rule:

Step 1: Give both the factor C and the LPH n small values.

Step 2: Increase the value of the factor C until the output tracking accuracy is satisfied.

Step 3: Increase the value of the LPH n to adjust the input amplitude.

D. STABILITY ANALYSIS

An important issue in system control is whether or not the closed-loop system under the derived control law is stable. In this subsection, stability analysis of the control law (15) is given in Theorem 4. Its proof is given in Appendix E.

Theorem 4: The plant (4) is controlled using predictive optimal control law (15) for the regulator $Y_d(k+1) = Y^* = [y^*_{1d}, \cdots, y^*_{md}]^T$ = constant vector. There always exists a positive definite diagonal matrix C making:

1) The system tracking error is convergent and $\lim_{k\to\infty} \|Y^* - Y(k+1)\|_v = 0$;
2) The closed-loop system is bounded-input-bounded-output (BIBO).

V. PLANT MODEL AND PROBLEM PROPOSITIO

In this paper, two assumptions are made for the quad-rotor: (1) the quad-rotor is rigid such that its frame deformation can be neglected, (2) the quad-rotor flies in low speed such that the earth rotation can be ignored. Besides, to make the work easy understanding, the payload is assumed to be cubic as other shapes are similar with this case. A quad-rotor carrying payload is illustrated in Figure 8 which is given by:

In Figure 8, $\{O_B, X_B, Y_B, Z_B\}$ represents the body frame of the quad-rotor, where O_B is coincide with the gravitational

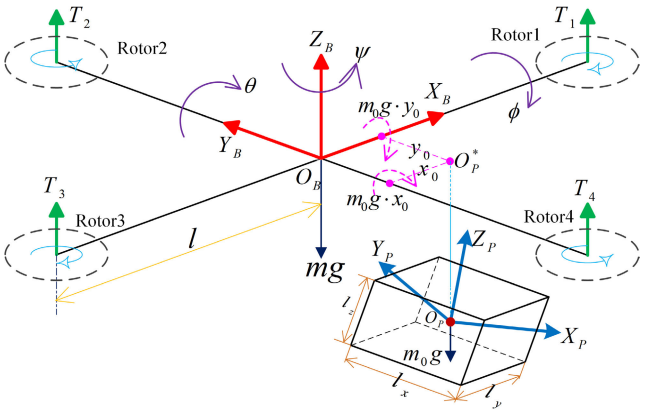

FIGURE 8. Sketch of the quad-rotor carrying payload using rigid connection.

center (GC) of the aircraft. $\{O_P, X_P, Y_P, Z_P\}$ represents the body frame of the payload, where O_P is coincide with the GC of the payload. $O_BX_BZ_B$ and $O_BY_BZ_B$ are the aircraft symmetrical planes. The distances between O_B and the projection points of the four rotor centers on $O_BX_BZ_B$ plane are the same and denoted as l. O_P is the GC of the payload. O_P^* is the projection point of O_P on $O_BX_BY_B$ plane with coordinate (x_0, y_0). x_0 and y_0 are eccentricities. m and m_0 are masses of the quad-rotor and the payload, respectively. T_i, $i = 1 \sim 4$ are thrusts of four rotors, respectively. l_x, l_y and l_z are geometrical parameters of the payload. The orientation of the aircraft is described by Euler angles $\Theta = [\phi, \theta, \psi]^T$. Assume that $\phi \in [-\pi/2, \pi/2]$ and $\theta \in [-\pi/2, \pi/2]$. Let $\Omega = [p, q, r]^T$ be the body rates. The inertia tensor of the aircraft with relative to the body frame is denoted as $J_q = diag(I_x, I_y, I_z)$.The moment of inertia of the payload with relative to the body frame is given by:

$$\Delta J = \begin{bmatrix} \Delta I_x & \Delta I_{xy} & \Delta I_{xz} \\ \Delta I_{xy} & \Delta I_x & \Delta I_{yz} \\ \Delta I_{xz} & \Delta I_{yz} & \Delta I_x \end{bmatrix} \quad (17)$$

To make the work practical, the payloads transported are assumed to be different (different shapes, sizes, masses, and eccentricities) in different stages. Hence, in mission execution, ΔJ can be regarded as slowly time-varying.

A. SYSTEM MODELLING

The kinematic model describes the relationship between the Euler angle vector and the body rate vector. In stable flight of the quad-rotor, the Euler angles and the body rates are small such that the kinematic model can be derived using a MIMO as:

$$\dot{\Theta} = \Omega \quad (18)$$

Denote $k_c > 0$ as a constant force-to-torque coefficient. According to Figure 8, the roll, pitch, and yaw torques M in body frame can be expressed as:

$$M = \begin{bmatrix} l(-T_1 + T_2 + T_3 - T_4) \\ l(-T_1 - T_2 + T_3 + T_4) \\ k_c(-T_1 + T_2 - T_3 + T_4) \end{bmatrix} \quad (19)$$

Take follow three virtual inputs:

$$\begin{cases} \tau_\phi = -T_1 + T_2 + T_3 - T_4 \\ \tau_\theta = -T_1 - T_2 + T_3 + T_4 \\ \tau_\psi = k_c(-T_1 + T_2 - T_3 + T_4) \end{cases} \tag{20}$$

By applying Newton-Euler method, the rotational dynamic model can be derived using a MIMO system as:

$$\left(J_q + \Delta J\right)\dot{\Omega} = -\Omega \times \left(J_q + \Delta J\right)\Omega + \Delta M + M \tag{21}$$

where, $\Delta M = [m_0 g \cdot y_0, m_0 g \cdot x_0, 0]^T$ are torque disturbances induced by the payload.

By recalling formulas (19) and (20), formula (21) can be written as:

$$\begin{aligned} \dot{\Omega} &= \left(J_q+\Delta J\right)^{-1}\left[-\Omega\times\left(J_q+\Delta J\right)\Omega+\Delta M\right] \\ &\quad +\left[\left(J_q+\Delta J\right)^{-1}-J_q^{-1}\right]\cdot M+J_q^{-1}\cdot M \\ &= \underbrace{\begin{array}{c}\left(J_q+\Delta J\right)^{-1}\left[-\Omega\times\left(J_q+\Delta J\right)\Omega+\Delta M\right] \\ +\left[\left(J_q+\Delta J\right)^{-1}-J_q^{-1}\right]\cdot M\end{array}}_{F_a=F_a(\Omega;\Delta J,m_0,x_0,y_0)} \\ &\quad +\underbrace{diag({}^{1}\!/_{I_x},\,{}^{1}\!/_{I_y},\,{}^{1}\!/_{I_z})}_{B_a}\cdot\underbrace{[\tau_\phi,\tau_\theta,\tau_\psi]^T}_{U_a} \\ &= F_a + B_a \cdot U_a \end{aligned} \tag{22}$$

It can be seen that $F_a = [F_a(1), F_a(2), F_a(3)]^T$ includes all aforementioned persistent disturbances.

The rotational movement of quad-rotor carrying payloads are expressed by formulas (18) and (22).

Remark 5: I_x, I_y, and I_z can be measured through cycloid method. We can see from Figure 8 and system (22) that the uncertainties caused by the payload are relative to ΔJ, (x_0, y_0), and m_0. It is easy to get intuitive understanding of (x_0, y_0) and m_0. While factors affecting ΔJ are complicated. For simplicity, we take ΔI_x in formula (17) as example to introduce the payload characteristics that may bring influences, as analyses of other elements in formula (17) are similar. ΔI_x can be computed by $\Delta I_x = \int_{m_0} r_x^2 dm$. r_x represents the distance between dm and O_P, which is relative to the eccentricities (x_0, y_0) and the payload dimension (for example, side lengths of a cuboid or diameter of a sphere). To sum up, ΔJ is relative to (x_0, y_0), m_0, and the payload dimension. In the simulation, we can measure the value of ΔJ in CATIA (a kind of computer aided design software) environment when (x_0, y_0), m_0, and the payload dimension are given.

B. PROBLEM PROPOSITIO

It is easy to verify that the quad-rotor attitude system given by formulas (18) and (22) satisfies A1 and A2. Then the problems need to be addressed here are stated as:

1. Use the DE proposed in formula (7) to estimate the nonlinear term $F_a = [F_a(1), F_a(2), F_a(3)]^T$ for compensation such that the attitude system robustness against disturbances from the unknown payloads can be enhanced.
2. Design predictive optimal controllers shown in formula (15) for the quad-rotor to degrade influences caused by sudden changes from payloads and prescribed references.

VI. CONTROL SCHEME DESIG

In this part, the proposed DE and POC are applied to control the quad-rotor in the application of payload transportation.

Denote $\Theta_d = [\phi_d, \theta_d, \psi_d]^T$ as the reference Euler angle vector and $\Omega_d = [p_d, q_d, r_d]^T$ as the desired body rate vector. To estimate $F_a(\Omega; \Delta J, m_0, x_0, y_0)$, we select the following nominal model:

$$\dot{\Omega}_m = B_a \cdot U_a \tag{23}$$

where, $\Omega_m(k) = [p_m(k), q_m(k), r_m(k)]^T$ is the state vector of the nominal model. It is obvious that B_a is a full rank square matrix.

Control structure of the proposed attitude control scheme is given by:

By recalling formula (7) and Appendix A, we can derive the estimation of F_a, namely $\widehat{F}_a$:

$$\begin{cases} \varepsilon(k) = \Omega(k) - \Omega_m(k) \\ \widehat{\Phi}_c(k) = \widehat{\Phi}_c(k-1) \\ \qquad + \dfrac{\eta[\Delta\varepsilon(k) - \widehat{\Phi}_c(k-1)\cdot\Delta U_a(k-1)]\Delta U_a^T(k-1)}{\mu + \|\Delta U_a(k-1)\|^2} \\ \widehat{F}_a(k) = \dfrac{\Delta\varepsilon(k)}{T} + \widehat{\Phi}_c(k)\cdot\Delta U_a(k) \end{cases} \tag{24}$$

Values of the parameters used in both Appendix A and formula (24) are given by: $\alpha = 1, b_1 = 10, \widehat{\Phi}_c(0) = diag(0.05, 0.05, 0.05), \eta = 1, \mu = 100$.

The POCs are given by:

(1) Euler angle control:

$$\begin{cases} \Omega_d(k) = (n_1 T \cdot C_1 + I)^{-1}\left[\overline{\Theta}_d(k+n_1) - C_1 \cdot \Theta(k)\right] \\ \overline{\Theta}_d(k+n_1) = (C_1 + \dfrac{1}{T}I)\Theta_d(k+n_1) - \dfrac{1}{T}\Theta_d(k+n_1-1) \end{cases} \tag{25}$$

(2) Body rate control:

$$\begin{cases} U_0(k) = [(n_2 T \cdot C_2 + I)B_a]^{-1} \\ \qquad \left[\overline{\Omega}_d(k+n_2) - C_2 \cdot \Omega(k)\right] \\ \overline{\Omega}_d(k+n_2) = (C_2 \\ \qquad + \dfrac{1}{T}I)\Omega_d(k+n_2) - \dfrac{1}{T}\Omega_d(k+n_2-1) \\ U_a(k) = U_0(k) - B_a^{-1}\cdot\widehat{F}_a(k) \end{cases} \tag{26}$$

VII. NUMERICAL VALIDATION

In this section, four application scenarios are simulated in the MATLAB environment. The first one validates effectiveness of the predictive function when the quad-rotor carrying an unknown unchanged payload tracks a piecewise step prescribed reference with sudden changes. In the second one,

we show the superiority of the proposed POC compared with the conventional PFC. In the third one, transporting unknown varying payloads using the quad-rotor with loading and dropping processes is simulated. Comparisons between the proposed scheme and the commonly used approaches such as the conventional SMC [8], cascade PID (CPID) [4], and FL [7] are carried out in order to show the superiority of the proposed scheme. In the last one, we consider more disturbances that the quad-rotor may encounter in the payload transportation missions.

Geometrical parameter values of the quad-rotor used in this paper are [10]: $m = 2kg, g = 9.81m \cdot s^{-2}, l = 0.35m, I_x = I_y = 1.25kg \cdot m^2, I_z = 2.5kg \cdot m^2, k_c = 0.035$.

The initial conditions are given by:

$$\begin{cases} (\phi, \theta, \psi \,|p, q, r)_0^T = (0, 0, 0|0, 0, 0)^T \\ (p_m, q_m, r_m)_0^T = (0, 0, 0)^T \end{cases} \tag{27}$$

Three types of payloads are delivered by the quad-rotor. Payload mass m_0(unit: kg), eccentricities (x_0, y_0)(unit: m), and the inertia tensor ΔJ(unit: $kg \cdot m^2$) are given by:

$$\begin{aligned} \text{P1}: (x_0, y_0) &= (0.1, 0.1)\,, m_0 = 1, \\ \Delta J &= \begin{bmatrix} 0.014 & -0.01 & 0.005 \\ -0.01 & 0.014 & 0.005 \\ 0.005 & 0.005 & 0.022 \end{bmatrix}; \\ \text{P2}: (x_0, y_0) &= (-0.15, 0.08)\,, m_0 = 0.8, \\ \Delta J &= \begin{bmatrix} 0.007 & 0.01 & -0.005 \\ 0.01 & 0.02 & 0.003 \\ -0.005 & 0.003 & 0.024 \end{bmatrix}; \\ \text{P3}: (x_0, y_0) &= (-0.18, -0.14)\,, m_0 = 1.2, \\ \Delta J &= \begin{bmatrix} 0.03 & -0.03 & -0.013 \\ -0.03 & 0.046 & -0.01 \\ -0.013 & -0.01 & 0.064 \end{bmatrix}. \end{aligned}$$

Remark 6: Values of m_0 and ΔJ are also measured in the CATIA environment. By referring to Figure 8, coordinates of the projection points $O_P^*(x_0, y_0)$ of the three payloads are in different quadrants. This aims to simulate different disturbance torques from different directions such that system robustness of the quad-rotor against disturbances induced by the payloads can be guaranteed.

The simulation step size $T = 0.002$ second is used in the next four application scenarios.

A. APPLICATION SCENARIO 1

The piecewise step prescribed reference (unit: rad) is given by:

$$\Theta_d = \begin{cases} [0.1, 0.2, \pi/6]^T, & t \le 3s \\ [0.3, 0.4, \pi/4]^T, & 3s < t \le 6s \end{cases} \tag{28}$$

In this case, only the payload P3 is carried by the quad-rotor.

This simulation experiment shows how the penalty factors C_1 and C_2(see formulas (25) and (26)) affect the control performance. Effects from the LPH are neglected since they have been discussed in [60] in detail. Values of the LPHs are given by: $n_1 = 10, n_2 = 10$.

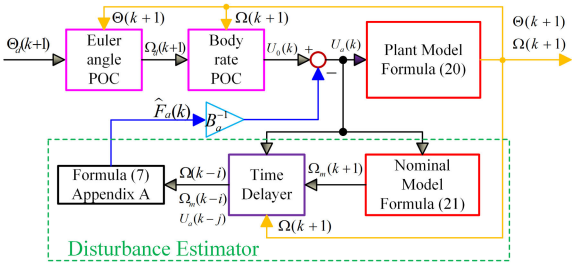

FIGURE 9. Control structure of the proposed quad-rotor attitude control scheme for payload transportation. *i* and *j* are time-delayed steps.

Simulation results are given by:

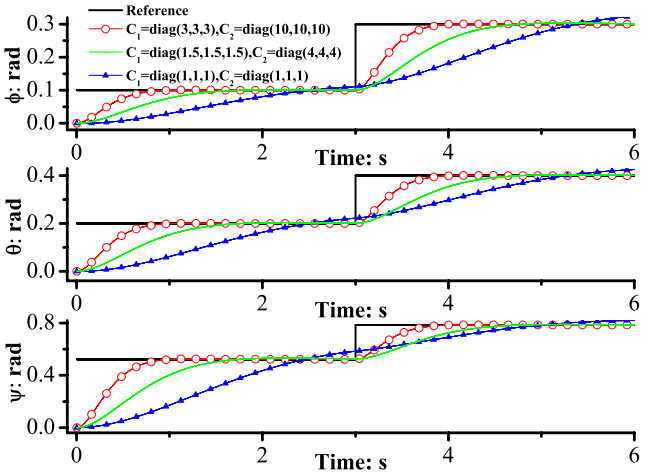

FIGURE 10. Euler angle responses with different penalty factors.

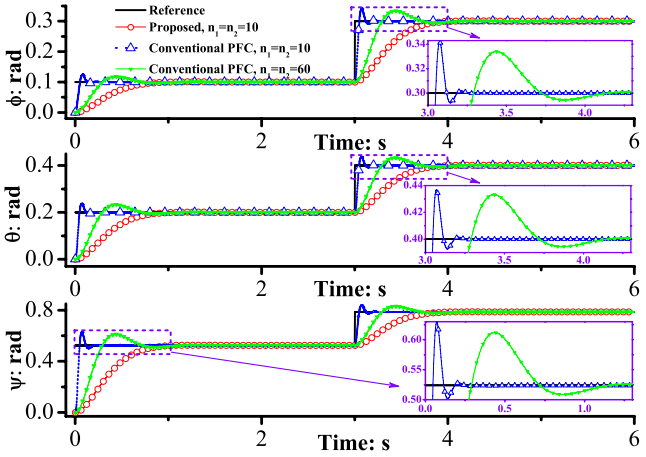

FIGURE 11. Comparisons between the schemes with and without the penalty factor: Euler angle responses.

Figure10 reveals that the Euler angle responses with large C_1 and C_2(the red solid line with hollow circle) have faster convergent speed than the ones with small C_1 and C_2(the blue solid line with solid triangle and the green solid line). Moreover, the three red solid lines with hollow circle show that when the reference signals change at $t = 3s$, the Euler

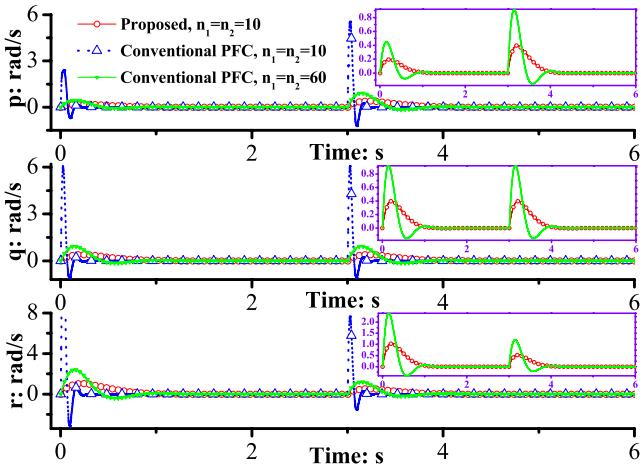

FIGURE 12. Comparisons between the schemes with and without the penalty factor: body rates.

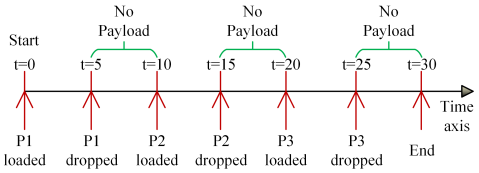

FIGURE 13. Simulation procedures for different payloads transportation.

angle responses have no overshoots since the LPH and the penalty factor together soften the system input signals which cannot surge instantly, causing overshoot phenomenon.

B. APPLICATION SCENARIO 2

In this subsection, we aim to show the superiority of the proposed controller compared with the conventional PFC. According to formula (13), the conventional PFCs for the quad-rotor transporting payloads control are given by:

(1) Euler angle control:

$$\Omega_d(k) = \frac{\Theta_d(k+n_1) - C_1 \cdot \Theta(k)}{n_1 T} \tag{29}$$

(2) Body rate control:

$$\begin{cases} U_0(k) = (n_2 T \cdot B_a)^{-1} \left[\Omega_d(k+n_2) - C_2 \cdot \Omega(k)\right] \\ U_a(k) = U_0(k) - B_a^{-1} \cdot \widehat{F}_a(k) \end{cases} \tag{30}$$

The prescribed reference is the same with (28). Parameters $C_1 = diag(3, 3, 3)$ and $C_2 = diag(10, 10, 10)$ are used in formulas (25) and (26). The payload P3 is carried by the quad-rotor. Contrast results are given by:

It is clear from the two figures that the proposed control scheme is superior to the conventional PFC in dealing with sudden changes in two aspects:

(1) Under the conditions of the same LPHs, output of the conventional PFC responds too fast at $t = 0$ and $t = 3$ such that too large overshoot and body rates are induced (see the blue line). However, in the proposed scheme (see the red line), by introducing the parameter C, the output errors and their changing rates are not allowed to change too fast such that the Euler angles and the body rates cannot change severely, which in turn avoids overshoot successfully.

(2) Though by setting $n_1 = n_2 = 60$(the predictive period is only 0.12 second) in the conventional PFC such that the quad-rotor system can have the same response time using the two controllers, the conventional PFC still has larger overshoot and much bigger amplitudes of the body rates than the proposed controller. The reason is that the conventional PFC ignores the changing rate of the output response speed.

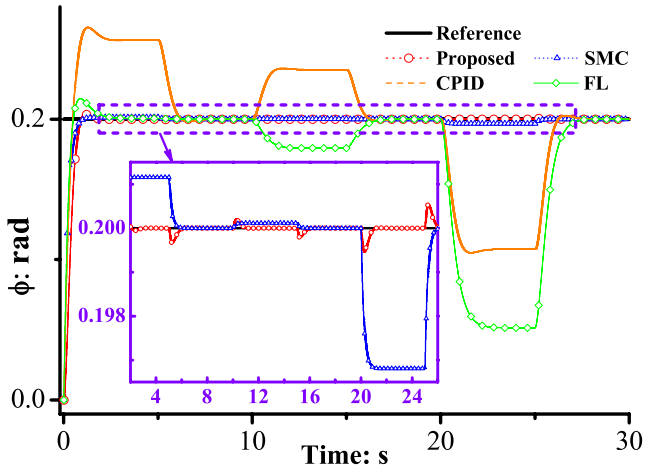

FIGURE 14. Roll angle responses.

C. APPLICATION SCENARIO 3

In this subsection, the quad-rotor transporting different payloads is simulated. The prescribed reference (unit: rad) is given by:

$$\Theta_d = [0.2, 0.2, 0.2]^T \tag{31}$$

Procedures of the quad-rotor loading and dropping the payloads are illustrated as:

Values of parameters in formulas (25) and (26) are given by: $n_1 = 10, C_1 = diag(3, 3, 3), n_2 = 10, C_2 = diag(10, 10, 10)$.

Simulation results are given by:

Conclusions can be drawn in three aspects:

(1) Figure 14∼ Figure 18 reveal that the proposed control scheme is superior to the one based on CPID and FL. Although the SMC-based scheme can achieve the same control performance with the proposed scheme, Figure 18 shows chattering phenomenon, which may damage the actuator. The superiority relies on the existence of the proposed DE which can estimate the disturbances (see Figure 17) for compensation without the availability of the amplitude UBs of the disturbances.

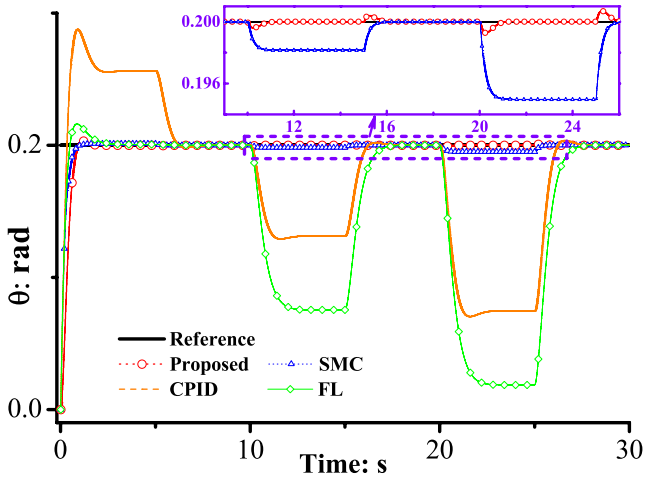

FIGURE 15. Pitch angle responses.

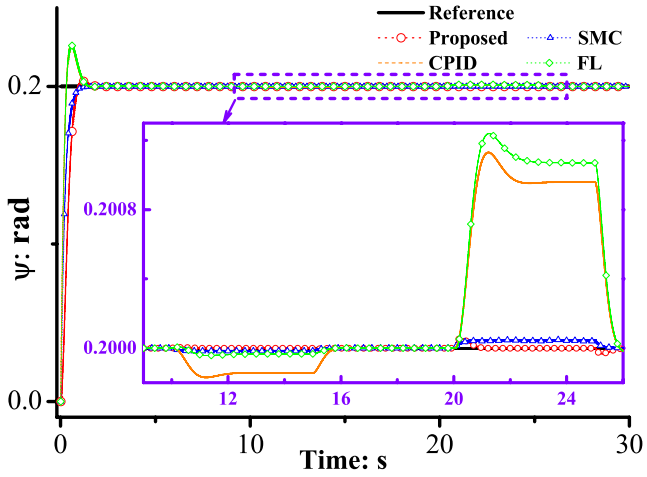

FIGURE 16. Yaw angle responses.

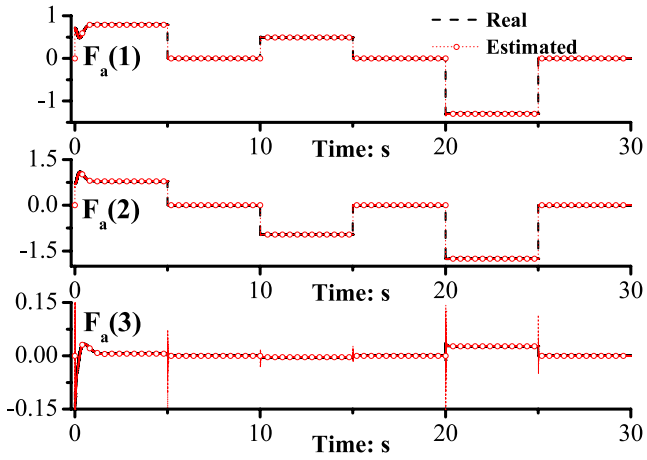

FIGURE 17. Estimation of F_a by the proposed DE.

(2) Figure 17 illustrates that the DE proposed can achieve high accuracy on estimation of the signals that have non-smooth points.

(3) From Figure 18 and the three enlarged figures in Figure 14∼ Figure 16, it can be seen that the proposed POC can degrade influences from the sudden changes since no input surging occurs (see Figure18) and the amplitudes of output fluctuations are very small.

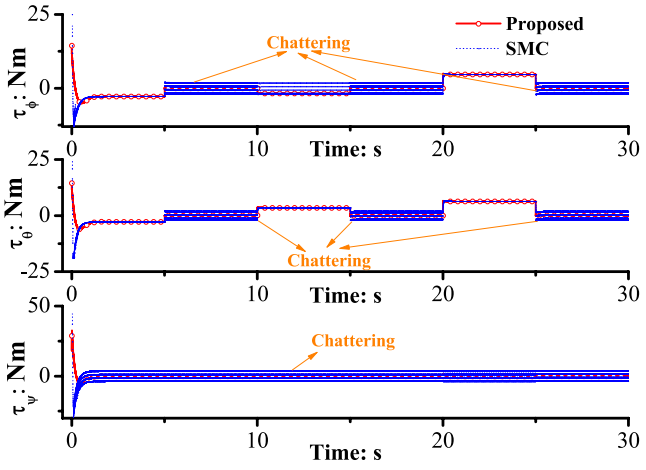

FIGURE 18. Control inputs.

D. APPLICATION SCENARIO 4

After demonstrating the superiority of the proposed control scheme, we consider more practical disturbances that the quad-rotor may encounter during the transportation period. That is, the unmodeled dynamics F_u, the sudden changes F_s from external circumstance, and the parameter perturbations. They are part of the unknown term F_a in formula (22). That is,

$$F_a = \left(J_q + \Delta J\right)^{-1}\left[-\Omega \times \left(J_q + \Delta J\right)\Omega + \Delta M\right] + \left[\left(J_q + \Delta J\right)^{-1} - J_q^{-1}\right] \cdot M + F_u + F_s \quad (32)$$

The unmodeled dynamics used here are given by [10]:

$$F_u = \begin{bmatrix} sign(\sin(0.9t)) \\ sign(\sin(0.9t)) + \cos(0.3t) \\ 0.5sign(\sin(0.5t)) + \cos(0.3t) + 2\cos(0.9t) \end{bmatrix} \quad (33)$$

The sudden changes are simulated by trigonometric functions, which are given by:

$$F_s = \begin{cases} \begin{bmatrix} 3\cos(\omega_0(t - \frac{5}{12}t_f)) \\ -3\cos(\omega_0(t - \frac{5}{12}t_f)) \\ 6\sin(\omega_0(t - \frac{5}{12}t_f)) \end{bmatrix}, & \frac{5}{12}t_f \le t \le \frac{5}{12}t_f + 2T \\ \begin{bmatrix} 3\cos(\omega_0(t - \frac{9}{12}t_f)) \\ -3\cos(\omega_0(t - \frac{9}{12}t_f)) \\ 6\sin(\omega_0(t - \frac{9}{12}t_f)) \end{bmatrix}, & \frac{9}{12}t_f \le t \le \frac{9}{12}t_f + 2T \end{cases} \quad (34)$$

where, $t_f = 30$ is the simulation time, $T = 0.002$ is the simulation step size, $\omega_0 = \pi/T$.

Notice that the geometrical parameter B_a in formulation (22) is used to design control law (26). However, there

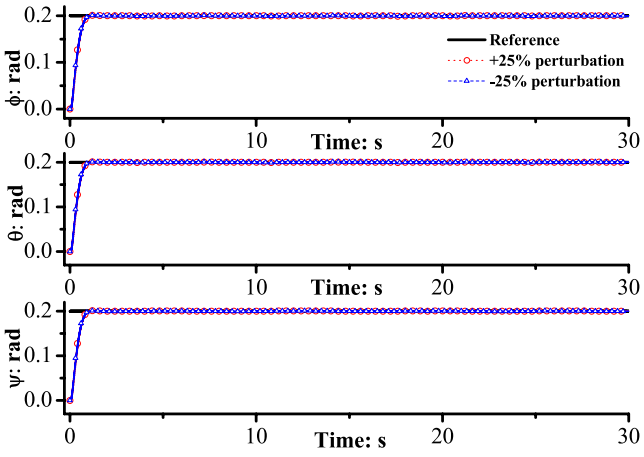

FIGURE 19. Euler angle responses.

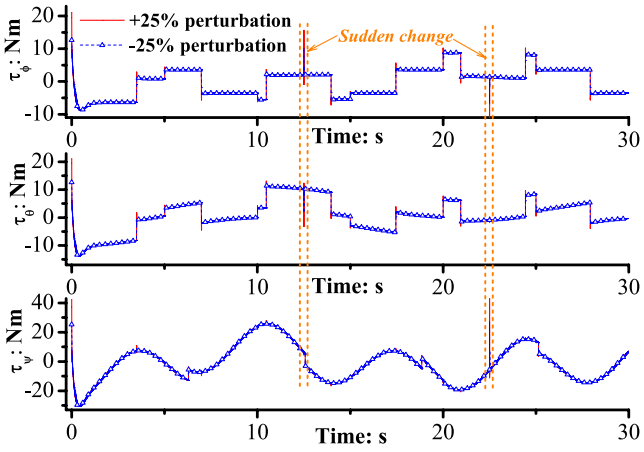

FIGURE 20. Control inputs.

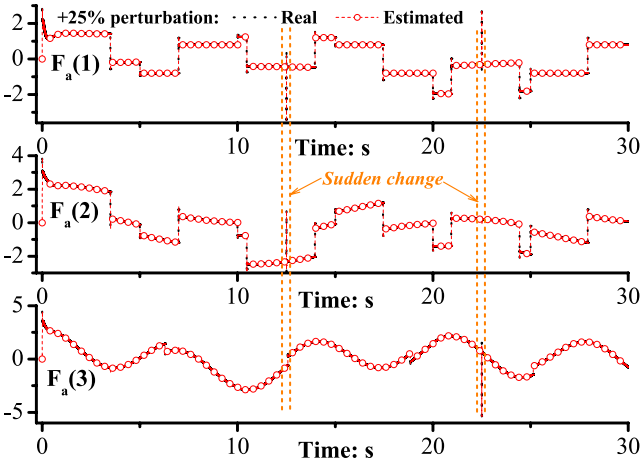

FIGURE 21. Estimation of F_a by the proposed DE: +25 perturbation.

always exists errors between the real value and the usage value. Here we assume that there exists $+25\%$ and -25% perturbations for B_a, respectively. Since we still use B_a to design the control law (26), thus, the real values of unknown disturbances caused by parameter perturbations included in F_a are given by: $-0.25B_a \cdot U_a$ and $0.25B_a \cdot U_a$.

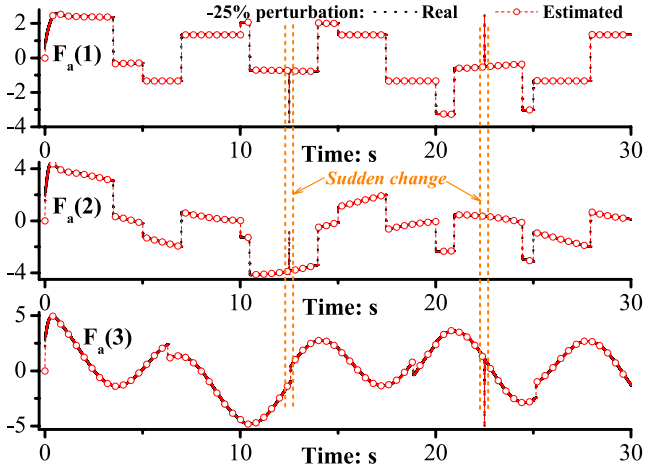

FIGURE 22. Estimation of F_a by the proposed DE: -25 perturbation.

Settings of all control parameters, the prescribed references, and the dropping/loading procedures are the same with the ones in scenario 3, subsection C. Simulation results are given by:

Conclusions of this scenario are given by:

Figure 19 reveals that, even under complicated flight circumstances, the proposed control scheme can guarantee the robustness of the quad-rotor system. Figure 20 illustrates that, input surging is avoided by the POC in the presence of sudden changes. Figures 21 and 22 illustrate that the proposed DE shows strong capability on the estimation of different disturbances.

VIII. CONCLUSION

This paper proposes a novel cascade control scheme with anti-disturbance capability and predictive optimal function to realize attitude control of quad-rotor delivering unknown payloads. Conclusions are drawn as follow:

1) The proposed DE orienting MIMO systems can estimate the uncertainties in an accurate manner at the non-smooth points, significantly enhancing system robustness of the quad-rotor against the payload disturbances, unmodeled dynamics, parameter perturbations, and external uncertainties. The DE proposed improves estimation accuracy and expands application ranges of the DOs.
2) The proposed predictive optimal controller can significantly degrade influences caused by the sudden changes from sudden loading/dropping of payloads and prescribed references by considering the changing rate of the output tracking error, which is superior to the conventional predictive functional controller.
3) Simulation results show that, the proposed control scheme is significantly superior to the ones based on sliding model control, cascade PID, and feedback linearization approaches, which are commonly used in flight control.

APPENDIX A
ONLINE ESTIMATION OF THE PJM [49]

PJM$\Phi_c(k)$ Online Estimation Scheme	
Updating law	$\widehat{\Phi}_c(k) = \widehat{\Phi}_c(k-1) + \frac{\eta\cdot[\Delta Y(k)-\widehat{\Phi}_c(k-1)\cdot\Delta U(k-1)]\Delta U^T(k-1)}{\mu+\|\Delta U(k-1)\|^2}$
Parameter setting	$\mu > 0, \eta \in (0,2], \widehat{\Phi}_c(k) = \left[\widehat{\phi}_{sn}(k)\right]_{m\times m}$
Resetting principle	$\widehat{\phi}_{ii}(k) = \widehat{\phi}_{ii}(0)$ if: $\left\|\widehat{\phi}_{ii}(k)\right\| < b_2$ or $\left\|\widehat{\phi}_{ii}(k)\right\| > \alpha b_2$ or $sign(\widehat{\phi}_{ii}(k)) \neq sign(\widehat{\phi}_{ii}(0)), i = 1,\cdots,m;$ $\widehat{\phi}_{ij}(k) = \widehat{\phi}_{ij}(0)$ if: $\left\|\widehat{\phi}_{ij}(k)\right\| > b_1$ or $sign(\widehat{\phi}_{ij}(k)) \neq sign(\widehat{\phi}_{ij}(0)),$ $i = 1,\cdots,m, j = 1,\cdots,m, i \neq j;$ $\widehat{\phi}_{ij}(0)$ is the initial value of $\widehat{\phi}_{ij}(k),$ $i = 1,\cdots,m, j = 1,\cdots,m;$ $\alpha \geq 1, b_2 > b_1(2\alpha+1)(m-1).$

APPENDIX B
PROOF OF THEOREM

Subtracting formula (5) from formula (4) yields:

$$\Sigma_2:\ \varepsilon(k+1) = \varepsilon(k) + T\cdot G(k) \tag{B1}$$

Moving $\varepsilon(k)$ to the left side yields:

$$\Sigma_2:\ \Delta\varepsilon(k+1) = T\cdot G(k) \tag{B2}$$

Then at $(k-1)T$, it has:

$$\Delta\varepsilon(k) = T\cdot G(k-1) \tag{B3}$$

Subtracting formula (B3) from formula (B2) yields:

$$\Delta\varepsilon(k+1) = \Delta\varepsilon(k) + T\cdot\Delta G(k) \tag{B4}$$

Applying Lemma 1 to linearize the system (B4) yields:

$$\Sigma_2:\ \Delta\varepsilon(k+1) = \Delta\varepsilon(k) + T\cdot\Phi_c(k)\cdot\Delta U(k) \tag{B5}$$

Finally, by making comparison between formulas (B2) and (B5), the disturbance term can be written as:

$$G(k) = \frac{\Delta\varepsilon(k)}{T} + \Phi_c(k)\cdot\Delta U(k) \tag{B6}$$

Using the algorithm in the Appendix A to estimate the PJM $\Phi_c(k)$ yields:

$$\widehat{G}(k) = \frac{\Delta\varepsilon(k)}{T} + \widehat{\Phi}_c(k)\cdot\Delta U(k) \tag{B7}$$

where, $\widehat{\Phi}_c(k)$ is a time-varying diagonally dominant matrix.

APPENDIX C
PROOF OF THEOREM 2

Here we only need to prove that the error between $\Phi_c(k)$ and $\widehat{\Phi}_c(k)$ is bounded.

Denote $\widehat{\Phi}_c(k) = [\widehat{\phi}_{c1}^T,\cdots,\widehat{\phi}_{cm}^T]^T$ and $\Phi_c(k) = [\phi_{c1}^T,\cdots,\phi_{cm}^T]^T$.

In resetting principles of the Appendix A, $\widehat{\Phi}_c(k)$ is obviously bounded. Thus, the estimation error is also bounded.

In other conditions, the estimation law for PJM can be rewritten as:

$$\begin{cases}\widehat{\phi}_{ci}(k) = \widehat{\phi}_{ci}(k-1) + \dfrac{\eta\cdot[\Delta y_i(k)-\widehat{\phi}_{ci}(k-1)\cdot\Delta U(k-1)]\Delta U^T(k-1)}{\mu+\|\Delta U(k-1)\|^2}\\ \Delta y_i(k) = \phi_{ci}(k-1)\cdot\Delta U(k-1)\end{cases} \tag{C1}$$

where, $i = 1,\cdots,m$. Denote $\widetilde{\phi}_{ci}(k) = \widehat{\phi}_{ci}(k) - \phi_{ci}(k)$. Subtracting the real value $\phi_{ci}(k)$ from both sides of formula (C1) yields:

$$\begin{aligned}&\widetilde{\phi}_{ci}(k)\\ &= \widehat{\phi}_{ci}(k-1) - \phi_{ci}(k)\\ &\quad + \frac{\eta[\Delta Y(k) - \widehat{\phi}_{ci}(k-1)\cdot\Delta U(k-1)]\Delta U^T(k-1)}{\mu+\|\Delta U(k-1)\|^2}\\ &= \widetilde{\phi}_{ci}(k-1) + \phi_{ci}(k-1) - \phi_{ci}(k)\\ &\quad - \frac{\eta\cdot\widetilde{\phi}_{ci}(k-1)\cdot\Delta U(k-1)\Delta U^T(k-1)}{\mu+\|\Delta U(k-1)\|^2}\\ &= \widetilde{\phi}_{ci}(k-1)\cdot[I - \frac{\eta\cdot\Delta U(k-1)\Delta U^T(k-1)}{\mu+\|\Delta U(k-1)\|^2}]\\ &\quad + \phi_{ci}(k-1) - \phi_{ci}(k)\end{aligned} \tag{C2}$$

where, I is an identity matrix with relative dimension.

Taking norm of both sides of formula (C2) and considering $\|\Phi_c(k)\| \leq b_c$ (implies $\|\phi_{ci}(k)\| \leq b_c$) yield:

$$\begin{aligned}&\left\|\widetilde{\phi}_{ci}(k)\right\|\\ &\leq \left\|\widetilde{\phi}_{ci}(k-1)[I - \frac{\eta\cdot\Delta U(k-1)\Delta U^T(k-1)}{\mu+\|\Delta U(k-1)\|^2}]\right\| + 2b_c\end{aligned} \tag{C3}$$

Besides, we have

$$\begin{aligned}&\left\|\widetilde{\phi}_{ci}(k-1)\cdot[I - \frac{\eta\cdot\Delta U(k-1)\Delta U^T(k-1)}{\mu+\|\Delta U(k-1)\|^2}]\right\|^2\\ &= \left\|\widetilde{\phi}_{ci}(k-1)\right\|^2 + [-2 + \frac{\eta\cdot\|\Delta U(k-1)\|^2}{\mu+\|\Delta U(k-1)\|^2}]\\ &\quad\cdot\frac{\eta\cdot\left\|\widetilde{\phi}_{ci}(k-1)\Delta U(k-1)\right\|^2}{\mu+\|\Delta U(k-1)\|^2}\end{aligned} \tag{C4}$$

By considering $\eta \in (0,2]$ and $\mu > 0$, we also have:

$$-2 + \frac{\eta\cdot\|\Delta U(k-1)\|^2}{\mu+\|\Delta U(k-1)\|^2} < 0 \tag{C5}$$

Formulas (C4) and (C5) means that there exists $0 < d_c < 1$ making the following work:

$$\left\|\widetilde{\phi}_{ci}(k-1)\cdot[I-\frac{\eta\cdot\Delta U(k-1)\Delta U^T(k-1)}{\mu+\|\Delta U(k-1)\|^2}]\right\| \leq d_c\left\|\widetilde{\phi}_{ci}(k-1)\right\| \quad \text{(C6)}$$

Here we only need to care about the existence of d_c instead of its specific value. Finally, we have:

$$\begin{aligned}\left\|\widetilde{\phi}_{ci}(k)\right\| &\leq d_c\left\|\widetilde{\phi}_{ci}(k-1)\right\| \\ &\quad +2b_c \leq d_c^2\left\|\widetilde{\phi}_{ci}(k-2)\right\|+2d_cb_c+2b_c \\ &\leq \cdots \leq d_c^k\left\|\widetilde{\phi}_{ci}(0)\right\|+\frac{2b_c(1-d_c^k)}{1-d_c}\end{aligned} \quad \text{(C7)}$$

Thus, the theorem is proved.

APPENDIX D
PROOF OF THEOREM 3

We consider the last two formulas in receding-horizon performance index:

$$\begin{cases} S(k+1)=C\cdot E(k+1)+\dfrac{E(k+1)-E(k)}{T} \\ E(k)=Y_d(k)-Y(k)\end{cases} \quad \text{(D1)}$$

By expanding $S(k+1)$, we have:

$$\begin{cases} S(k+1)=\dfrac{1}{T}Y(k)-(C+\dfrac{1}{T}I)Y(k+1)+\overline{Y}_d(k) \\ \overline{Y}_d(k)=(C+\dfrac{1}{T}I)Y_d(k+1)-\dfrac{1}{T}Y_d(k)\end{cases} \quad \text{(D2)}$$

where, $I \in R^{m\times m}$ is an identity matrix with relative dimension.

By recalling formula (12) and applying recursion method to formula (D2), we derive:

$$S(k+n|k)=-C\cdot Y(k)-(nT\cdot C+I)B_mU(k)+\overline{Y}_d(k+n|k) \quad \text{(D3)}$$

where,

$$\overline{Y}_d(k+n|k)=(C+\frac{1}{T}I)Y_d(k+n|k)-\frac{1}{T}Y_d(k+n-1|k) \quad \text{(D4)}$$

By bringing formulas (D3) and (D4) into $J(k)=\frac{1}{2}S^T(k+n|k)S(k+n|k)$ and letting $\partial J(k)/\partial U(k)=0$, the predictive optimal control law can be given by:

$$U(k)=[(nT\cdot C+I)B_m]^{-1}\left[\overline{Y}_d(k+n|k)-C\cdot Y(k)\right] \quad \text{(D5)}$$

$\overline{Y}_d(k+n|k)$ is given by formula (D4).

APPENDIX
PROOF OF THEOREM 4

Denote

$$E(k+1)=Y_d(k+1)-Y(k+1)=Y^*-Y(k+1) \quad \text{(E1)}$$

Bringing formulas (D4) and (D5) into (D1) and letting $n=1$ yield:

$$\begin{aligned}&E(k+1)\\ &=Y^*-Y(k)-T\cdot B_m\cdot[(nT\cdot C+I)B_m]^{-1}\\ &\quad\cdot\left[\overline{Y}_d(k+n)-C\cdot Y(k)\right]\\ &=E(k)-T\cdot(nT\cdot C+I)^{-1}\cdot\left[\overline{Y}_d(k+n)-C\cdot Y(k)\right]\\ &=\left[I-T\cdot(nT\cdot C+I)^{-1}\cdot C\right]E(k)\\ &=P\cdot E(k)\end{aligned} \quad \text{(E2)}$$

Let $C=diag(c_1,\cdots,c_m), c_i>0, i=1,\cdots,m$. Then it has $P=diag(p_1,\cdots,p_m)=diag(1-\frac{T\cdot c_1}{1+nT\cdot c_1},\cdots,1-\frac{T\cdot c_m}{1+nT\cdot c_m})$. It is easy to find that $0<p_i=1-\frac{T\cdot c_i}{1+nT\cdot c_i}<1, i=1,\cdots,m$. Denote $\rho=\max\{p_1,\cdots,p_m\}$.Thus, there exists a positive number d_1 and a small number ξ such that

$$0<\|P\|_v\leq\rho+\xi=d_1<1 \quad \text{(E3)}$$

Taking norm of both sides of formula (E2) and using (E3) yield:

$$\begin{aligned}\left\|Y^*-Y(k+1)\right\|_v&=\|E(k+1)\|_v\\ &\leq\|P\|_v\cdot\|E(k)\|_v\leq d_1\cdot\|E(k)\|_v\\ &\leq\cdots\leq d_1^{k+1}\cdot\|E(0)\|_v\end{aligned} \quad \text{(E4)}$$

Formula (E4) implies that $\lim_{k\to\infty}\|Y^*-Y(k+1)\|_v=0$, which also indicates that the output $Y(k+1)$ is bounded.

Meanwhile, formula (E4) implies that there exists a constant d_2 making $0<\|E(k)\|_v\leq d_2$.

Then in the predictive optimal control law (D4), it has

$$\begin{aligned}&\|U(k)\|_v\\ &\leq\left\|[(nT\cdot C+I)B_m]^{-1}\cdot\left[\overline{Y}_d(k+n)-C\cdot Y(k)\right]\right\|_v\\ &\leq\left\|[(nT\cdot C+I)B_m]^{-1}\cdot C\right\|_v\cdot\|E(k)\|_v\end{aligned} \quad \text{(E5)}$$

Notice that $[(nT\cdot C+I)B_m]^{-1}\cdot C$ is a constant matrix and recall that $0<\|E(k)\|_v\leq d_2$. We have $\|U(k)\|_v\leq M\cdot d_2=d_3$, which means that inputs of the system are bounded.

Thus, the BIBO of the closed-loop system is proved.

REFERENCES

[1] A. Poultney, P. Gong, and H. Ashrafiuon, "Integral backstepping control for trajectory and yaw motion tracking of quadrotors," *Robotica*, vol. 37, no. 2, pp. 300–320, 2019.
[2] S. Papatheodorou, A. Tzes, and Y. Stergiopoulos, "Collaborative visual area coverage," *Robot. Auto. Syst.*, vol. 92, pp. 126–138, Jun. 2017.
[3] S. Yang, S. A. Scherer, X. Yi, and A. Zell, "Multi-camera visual SLAM for autonomous navigation of micro aerial vehicles," *Robot. Auto. Syst.*, vol. 93, pp. 116–134, Jul. 2017.
[4] G. Bo, L. Xin, Z. Hui, and W. Ling, "Quadrotor helicopter attitude control using cascade PID," in *Proc. Chin. Control Decis. Conf. (CCDC)*, Yinchuan, China, May 2016, pp. 5158–5163.
[5] S. Bouabdallah, A. Noth, and R. Siegwart, "PID vs LQ control techniques applied to an indoor micro quadrotor," in *Proc. IEEE/RSJ Int. Conf. Intell. Robots Syst. (IROS)*, Sendai, Japan, Oct. 2004, pp. 2451–2456.
[6] Y. Zeng, Q. Jiang, Q. Liu, and H. Jing, "PID vs. MRAC control techniques applied to a quadrotor's attitude," in *Proc. 2nd Int. Conf. Instrum., Meas., Comput., Commun. Control*, Harbin, China, Dec. 2012, pp. 1086–1089.

[7] A. Jebelli, M. C. E. Yagoub, and B. S. Dhillon, "Feedback linearization approach to fault tolerance for a micro quadrotor," in *Proc. IEEE Int. Conf. Ind. Technol. (ICIT)*, Lyon, France, Feb. 2018, pp. 165–168.

[8] Y. Yang and Y. Yan, "Attitude regulation for unmanned quadrotors using adaptive fuzzy gain-scheduling sliding mode control," *Aerosp. Sci. Technol.*, vol. 54, pp. 208–217, Jul. 2016.

[9] C. Fu, W. Hong, H. Lu, L. Zhang, X. Guo, and Y. Tian, "Adaptive robust backstepping attitude control for a multi-rotor unmanned aerial vehicle with time-varying output constraints," *Aerosp. Sci. Technol.*, vol. 78, pp. 593–603, Jul. 2018.

[10] Y. Zhang, Z. Chen, X. Zhang, Q. Sun, and M. Sun, "A novel control scheme for quadrotor UAV based upon active disturbance rejection control," *Aerosp. Sci. Technol.*, vol. 79, pp. 601–609, Aug. 2018.

[11] L. Xu, D. Guo, and H. Ma, "Cascade active disturbance rejection control for quadrotor UAV," in *Proc. Chin. Control Conf. (CCC)*, Guangzhou, China, Jul. 2019, pp. 8044–8048.

[12] S. M. Orozco-Soto, P. Vera-Bustamante, and J. M. Ibarra-Zannatha, "ORB-SLAM based active disturbance rejection control for quadrotor autonomous flight," in *Proc. 20th Congreso Mexicano de Robótica (COMRob)*, Ensenada, Mexico, Sep. 2018, pp. 1–6.

[13] X. Liang, J. Li, and F. Zhao, "Attitude control of quadrotor UAV based on LADRC method," in *Proc. Chin. Control Decis. Conf. (CCDC)*, Nanchang, China, Jun. 2019, pp. 1924–1929.

[14] H. Yang, L. Cheng, Y. Xia, and Y. Yuan, "Active disturbance rejection attitude control for a dual closed-loop quadrotor under gust wind," *IEEE Trans. Control Syst. Technol.*, vol. 26, no. 4, pp. 1400–1405, Jul. 2018.

[15] J. Che, D. Li, Y. Ji, and Q. Gao, "Attitude control for a quadrotor base on ADRC with GSO parameter optimization," in *Proc. Chin. Control Decis. Conf. (CCDC)*, Shenyang, China, Jun. 2018, pp. 1364–1369.

[16] H. Liang, Y. Xu, and X. Yu, "ADRC vs LADRC for quadrotor UAV with wind disturbances," in *Proc. Chin. Control Conf. (CCC)*, Guangzhou, China, Jul. 2019, pp. 8037–8043.

[17] N. Wang, Q. Deng, H. Zhao, J. Yin, and Z. Zheng, "Nonlinear disturbance observer-based sliding backstepping hovering control of a quadrotor," in *Proc. Chin. Control Decis. Conf. (CCDC)*, Shenyang, China, Jun. 2018, pp. 3274–3279.

[18] W. Taha, A. Al-Durra, R. Errouissi, and K. Al-Wahedi, "Nonlinear disturbance observer-based control for quadrotor UAV," in *Proc. 44th Annu. Conf. IEEE Ind. Electron. Soc. (IECON)*, Washington, DC, USA, Oct. 2018, pp. 2589–2595.

[19] H. Ban, Z. Qi, B. Li, and W. Gong, "Nonlinear disturbance observer based dynamic surface control for trajectory tracking of a quadrotor UAV," in *Proc. Int. Symp. Sens. Instrum. IoT Era (ISSI)*, Shanghai, China, Sep. 2018, pp. 1–6.

[20] Z. He, Y. Fan, J. Cao, and G. Wang, "Disturbance observer based nonlinear control for a quadrotor trajectory tracking," in *Proc. Chin. Control Conf. (CCC)*, Guangzhou, China, Jul. 2019, pp. 581–587.

[21] C. C. Murray and A. G. Chu, "The flying sidekick traveling salesman problem: Optimization of drone-assisted parcel delivery," *Transp. Res. C, Emerg. Technol.*, vol. 54, pp. 86–109, May 2015.

[22] E. L. de Angelis, F. Giulietti, and G. Pipeleers, "Two-time-scale control of a multirotor aircraft for suspended load transportation," *Aerosp. Sci. Technol.*, vol. 84, pp. 193–203, Jan. 2019.

[23] E. L. de Angelis, "Swing angle estimation for multicopter slung load applications," *Aerosp. Sci. Technol.*, vol. 89, pp. 264–274, Jun. 2019.

[24] A. Faust, I. Palunko, P. Cruz, R. Fierro, and L. Tapia, "Learning swing-free trajectories for UAVs with a suspended load," in *Proc. IEEE Int. Conf. Robot. Autom.*, Karlsruhe, Germany, May 2013, pp. 4902–4909.

[25] G. Yu, D. Cabecinhas, R. Cunha, and C. Silvestre, "Nonlinear backstepping control of a quadrotor-slung load system," *IEEE/ASME Trans. Mechatronics*, vol. 24, no. 5, pp. 2304–2315, Oct. 2019.

[26] G. Wu and K. Sreenath, "Variation-based linearization of nonlinear systems evolving on *SO(3)* and $\mathbb{S}^2$," *IEEE Access*, vol. 3, pp. 1592–1604, 2015.

[27] S. Tang, V. Wuest, and V. Kumar, "Aggressive flight with suspended payloads using vision-based control," *IEEE Robot. Autom. Lett.*, vol. 3, no. 2, pp. 1152–1159, Apr. 2018.

[28] S. Dai, T. Lee, and D. S. Bernstein, "Adaptive control of a quadrotor UAV transporting a cable-suspended load with unknown mass," in *Proc. 53rd IEEE Conf. Decis. Control*, Los Angeles, CA, USA, Dec. 2014, pp. 6149–6154.

[29] X. Yuan, X. Ren, B. Zhu, Z. Zheng, and Z. Zuo, "Robust H∞ control for hovering of a quadrotor UAV with slung load," in *Proc. 12th Asian Control Conf. (ASCC)*, Kitakyushu-shi, Japan, Jun. 2019, pp. 114–119.

[30] L. Tan, Z. Shen, and S. Yu, "Adaptive fault-tolerant flight control for a quadrotor UAV with slung payload and varying COG," in *Proc. 3rd Int. Symp. Auto. Syst. (ISAS)*, Shanhai, China, May 2019, pp. 227–231.

[31] S. Wang and B. Xian, "An anti-swing trajectory approach for an unmanned aerial vehicle with a slung payload," in *Proc. 37th Chin. Control Conf. (CCC)*, Wuhan, China, Jul. 2018, pp. 5560–5565.

[32] X. Huo, J. Y. Chen, Q. Q. Liu, and X. He, "Vibration elimination for quadrotor slung system based on input shaping and double closed-loop control," in *Proc. 12th Asian Control Conf. (ASCC)*, Kitakyushu-shi, Japan, Jun. 2019, pp. 492–497.

[33] M. Vahdanipour and M. Khodabandeh, "Adaptive fractional order sliding mode control for a quadrotor with a varying load," *Aerosp. Sci. Technol.*, vol. 86, pp. 737–747, Mar. 2019.

[34] B. Wang, L. Mu, and Y. Zhang, "Adaptive robust control of quadrotor helicopter towards payload transportation applications," in *Proc. 36th Chin. Control Conf. (CCC)*, Dalian, China, Jul. 2017, pp. 4774–4779.

[35] I. Sadeghzadeh, M. Abdolhosseini, and Y. M. Zhang, "Payload drop application of unmanned quadrotor helicopter using gain-scheduled PID and model predictive control techniques," in *Proc. 5th Int. Conf. Intell. Robot. Appl.*, Montreal, QC, Canada, Oct. 2012, pp. 386–395.

[36] A. K. Shastry, M. T. Bhargavapuri, M. Kothari, and S. R. Sahoo, "Quaternion based adaptive control for package delivery using variable-pitch quadrotors," in *Proc. Indian Control Conf. (ICC)*, Kanpur, India, Jan. 2018, pp. 340–345.

[37] G. N. P. Pratama, I. Masngut, A. I. Cahyadi, and S. Herdjunanto, "Robustness of PD control for transporting quadrotor with payload uncertainties," in *Proc. 3rd Int. Conf. Sci. Technol.-Comput. (ICST)*, Yogyakarta, Indonesia, Jul. 2017, pp. 11–15.

[38] D. W. Kun and I. Hwang, "Linear matrix inequality-based nonlinear adaptive robust control of quadrotor," *J. Guid., Control, Dyn.*, vol. 39, no. 5, pp. 996–1008, May 2016.

[39] D. Mellinger, M. Shomin, N. Michael, and V. Kumar, "Cooperative grasping and transport using multiple quadrotors," in *Distributed Autonomous Robotic Systems*, vol. 83. Berlin, Germany: Springer, 2013, pp. 545–558.

[40] H. Durrant-Whyte, and N. RoyP. Abbeel, "Construction of cubic structures with quadrotor teams," in *Robotics: Science and Systems VII*. Cambridge, MA, USA: MIT Press, 2012, pp. 177–184.

[41] S. Kim, S. Choi, and H. J. Kim, "Aerial manipulation using a quadrotor with a two DOF robotic arm," in *Proc. IEEE/RSJ Int. Conf. Intell. Robots Syst.*, Tokyo, Japan, Nov. 2013, pp. 4990–4995.

[42] O. Garcia, P. Ordaz, O.-J. Santos-Sanchez, S. Salazar, and R. Lozano, "Backstepping and robust control for a quadrotor in outdoors environments: An experimental approach," *IEEE Access*, vol. 7, pp. 40636–40648, 2019.

[43] J. Sun, Y. Wang, Y. Yu, and C. Sun, "Nonlinear robust compensation method for trajectory tracking control of quadrotors," *IEEE Access*, vol. 7, pp. 26766–26776, 2019.

[44] H. Chang, Y. Liu, Y. Wang, and X. Zheng, "A modified nonlinear dynamic inversion method for attitude control of UAVs under persistent disturbances," in *Proc. IEEE Int. Conf. Inf. Autom. (ICIA)*, Macau, China, Jul. 2017, pp. 715–721.

[45] Z. Wang, J. Yu, S. Lin, J. Dong, and Z. Yu, "Distributed robust adaptive fault-tolerant mechanism for quadrotor UAV real-time wireless network systems with random delay and packet loss," *IEEE Access*, vol. 7, pp. 134055–134062, 2019.

[46] B. Tian, Y. Ma, and Q. Zong, "A continuous finite-time output feedback control scheme and its application in quadrotor UAVs," *IEEE Access*, vol. 6, pp. 19807–19813, 2018.

[47] J. De Jesus Rubio, J. F. Novoa, G. Ochoa, D. Mujica-Vargas, E. Garcia, R. Balcazar, I. Elias, D. R. Cruz, C. F. Juarez, and A. Aguilar, "Structure regulator for the perturbations attenuation in a quadrotor," *IEEE Access*, vol. 7, pp. 138244–138252, 2019.

[48] M. Labbadi and M. Cherkaoui, "Robust adaptive backstepping fast terminal sliding mode controller for uncertain quadrotor UAV," *Aerosp. Sci. Technol.*, vol. 93, Oct. 2019, Art. no. 105306.

[49] Z. S. Hou and S. T. Jin, *Model Free Adaptive Control: Theory and Applications*. Boca Raton, FL, USA: CRC Press, 2013, pp. 64–66.

[50] S. H. Li, J. Yang, W. H. Chen, and X. S. Chen, *Disturbance Observer-Based Control: Methods and Applications*. Boca Raton, FL, USA: CRC Press, 2014, pp. 43–158.

[51] B. A. Güvenç, L. Güvenç, and S. Karaman, "Robust MIMO disturbance observer analysis and design with application to active car steering," *Int. J. Robust Nonlinear Control*, vol. 20, pp. 873–891, May 2010.

[52] M. Demirci and M. Gokasan, "MIMO disturbance observer for input-output decoupling with application to 4WAS vehicles," in *Proc. IEEE Int. Conf. Mechatronics*, İstanbul, Turkey, Apr. 2011, pp. 90–95.
[53] E. Kim and S. Lee, "Output feedback tracking control of MIMO systems using a fuzzy disturbance observer and its application to the speed control of a PM synchronous motor," *IEEE Trans. Fuzzy Syst.*, vol. 13, no. 6, pp. 725–741, Dec. 2005.
[54] J. Han, "From PID to active disturbance rejection control," *IEEE Trans. Ind. Electron.*, vol. 56, no. 3, pp. 900–906, Mar. 2009.
[55] W.-H. Chen, "Nonlinear disturbance observer-enhanced dynamic inversion control of missiles," *J. Guid., Control, Dyn.*, vol. 26, no. 1, pp. 161–166, Jan. 2003.
[56] B. B. Kocer, T. Tjahjowidodo, and G. G. L. Seet, "Centralized predictive ceiling interaction control of quadrotor VTOL UAV," *Aerosp. Sci. Technol.*, vol. 76, pp. 455–465, May 2018.
[57] M. Montazeri-Gh, A. Rasti, A. Jafari, and M. Ehteshami, "Design and implementation of MPC for turbofan engine control system," *Aerosp. Sci. Technol.*, vol. 92, pp. 99–113, Sep. 2019.
[58] M. Mammarella, E. Capello, H. Park, G. Guglieri, and M. Romano, "Tube-based robust model predictive control for spacecraft proximity operations in the presence of persistent disturbance," *Aerosp. Sci. Technol.*, vol. 77, pp. 585–594, Jun. 2018.
[59] X. Liu, Q. Sun, and J. E. Cooper, "LQG based model predictive control for gust load alleviation," *Aerosp. Sci. Technol.*, vol. 71, pp. 499–509, Dec. 2017.
[60] J. A. Rossiter, "A priori stability results for PFC," *Int. J. Control*, vol. 90, no. 2, pp. 289–297, 2017.
[61] Z. Hou, S. Liu, and T. Tian, "Lazy-learning-based data-driven model-free adaptive predictive control for a class of discrete-time nonlinear systems," *IEEE Trans. Neural Netw. Learn. Syst.*, vol. 28, no. 8, pp. 1914–1928, Aug. 2017.
[62] Q. Jia, W. Zhang, J. Shi, and J. Hu, "Maneuverable aircraft flight control using nonlinear dynamic inversion," in *Proc. 18th Int. Conf. Control, Autom. Syst. (ICCAS)*, Gangwon-do, South Korea, Oct. 2018, pp. 1513–1518.
[63] J. Liu and J. Yang, "Spacecraft high accuracy attitude control by quaternion-based nonlinear dynamic inversion," in *Proc. Chin. Control Conf. (CCC)*, Guangzhou, China, Jul. 2019, pp. 656–661.
[64] Y. Li, W. Zhang, and J. Shi, "Super-maneuver control of thrust vector aircraft based on nonlinear dynamic inversion," in *Proc. Chin. Control Conf. (CCC)*, Guangzhou, China, Jul. 2019, pp. 656–661.
[65] M. L. Chen and Y. Wang, "An improved nonlinear dynamic inversion method for altitude and attitude control of nano quad-rotors under persistent uncertainties," Trans. Nanjing Univ. Aeronaut. Astronaut., Nanjing, China, Tech. Rep. 3, 2018, vol. 35, no. 3, pp. 93–103.
[66] J. Richalet and D. O. Donovan, *Predictive Functional Control: Principles and Industrial Applications* (Advances in Industrial Control). Berlin, Germany: Springer, 2009, pp. 18–20.

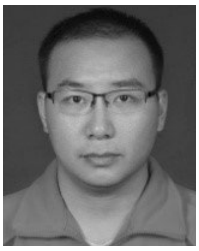

YUAN WANG received the M.Sc. degree in aerospace engineering from the Nanjing University of Aeronautics and Astronautics, Nanjing, China, in 2015, where he is currently pursuing the Ph.D. degree in aircraft design.

His research is focused on nonlinear control theories and their applications on fixed-wing, multi-rotor, and tilt rotor UAVs.

HONGMING CAI received the Ph.D. degree in aircraft design from the Nanjing University of Aeronautics and Astronautics, Nanjing, China, in 2012. He is currently with the Nanjing University of Science and Technology.

His researches are focused on aircraft design, aerodynamics, and flight control.

JUNMIAO ZHANG received the Ph.D. degree in mechanical design and theory from the Nanjing University of Aeronautics and Astronautics, Nanjing, China, in 2013. He is currently teaching at the Jiangsu University of Science and Technology.

His research has focused on electronic control systems in mechanical and electrical engineering.

XUBO LI received the M.Sc. degree in aerospace engineering from the Nanjing University of Aeronautics and Astronautics, Nanjing, China, in 2017, where he is currently pursuing the Ph.D. degree in aircraft design.

His research is focused on landing gear dynamics and control.